Biosurface and Biotribology

Review Article

IET Journals
The Institution of Engineering and Technology

Enhanced flow sensing with interfacial microstructures

ISSN 2405-4518
Received on 29th November 2019
Revised on 13th January 2020
Accepted on 7th February 2020
doi: 10.1049/bsbt.2019.0043
www.ietdl.org

Yonggang Jiang[1,2] ✉, Peng Zhao[1], Zhiqiang Ma[1], Dawei Shen[1], Gongchao Liu[1], Deyuan Zhang[1]

[1]*Institute of Bionic and Micro-Nano Systems, School of Mechanical Engineering and Automation, Beihang University, Beijing 100191, People's Republic of China*
[2]*International Research Institute of Multidisciplinary Science, Beihang University, Beijing 100191, People's Republic of China*
✉ *E-mail: jiangyg@buaa.edu.cn*

Abstract: Biological flow receptors show astonishing performance and are used as models for the design of novel flow sensors. However, the functional importance of interfacial microstructures is seldom discussed in previous review papers. Herein, this review summarises the underlying biomechanical principles in the biological flow receptors and describes the recent progress in bio-inspired flow sensors, in which the underlying sensing-enhancement mechanisms are emphasised.

1 Introduction

Flow perception plays an important role in the many behaviours of flying and aquatic animals, as fluid dynamic stimuli provide an important source of external information. For instance, the lateral-line system of fish, which is able to perceive the surrounding weak flow and pressure variations, contributes to various functions such as rheotaxis, schooling, prey detection, navigation and communication [1]. The flow receptor systems display a striking morphological diversity, which ranges from feather follicles on the avian wings [2], filiform hair in insects [3], Johnston organs of Whirligig beetles [4], whiskers of harbour seals [5], and lateral-line system of fish [6].

The flow sensory functions are strongly correlated with the morphology of flow receptors. Fratzl and Barth [7] described the trichobothria in spider with a remarkable sensitivity, which is due to the lever system in the flow-sensing organ. In addition, feathered hair on the outer arm of trichobothria can greatly increase the drag force and thus the flow sensitivity [8]. Dehnhardt *et al.* [9] showed that harbour seals can use their whiskers to detect minute water movement resulting from other aquatic animals. Hanke *et al.* [10] further discovered that the undulated structure of seal whisker could effectively change the vortex street and suppress the vibration induced by the shedding of vortices from the whiskers, thus improving the flow-sensing performance. Constriction microstructures were discovered in the lateral-line canals of fish to enhance the sensitivity in the detection of pressure disturbance and modify the frequency response of the canal lateral-line system [11]. Though there are many review papers on the different flow reception systems [12–14], few literature put an emphasis on the detailed interfacial structures of flow receptors and the underlying sensing-enhancement mechanisms, which might shed light on the potential biomimetic design of flow sensors.

In this review, we will focus on the biological flow reception systems with specialised interfacial structures, and the sensing-enhancement mechanisms based on the morphology of flow receptors. The recent progress in bio-inspired flow-sensing systems will be discussed in detail.

2 Sensing-enhancement mechanisms in biological flow receptors

The aquatic and flying animals exhibit various flow receptors, which evolved with specialised interfacial microstructures to improve the flow-sensing performance, for living in complex fluidic environments. This section describes several examples of biological flow receptors with interesting sensing-enhancement mechanisms.

2.1 Lateral line of fish

Fish and aquatic amphibians are able to perceive minute fluid motions and pressure gradients with their mechanosensory lateral-line system [15, 16]. Inspired by the fish lateral-line system, researchers have proposed various artificial lateral line (ALL) sensors based on different sensing mechanisms [1]. However, the sensing performance of the ALL sensors scarcely matches the performance of their biological prototypes. It is desirable to understand sensing-enhancement mechanisms in the lateral-line system to develop highly sensitive flow sensors.

2.1.1 Cupula microstructure: The lateral line is composed of numerous neuromasts, within which tens of hair cells are covered by a soft gelatinous structure, called cupula (Fig. 1*a*) [17]. The cupula couples the mechanosensory hair cells to the surrounding water. Teyke [18] found that the cephalic cupula heights of superficial neuromasts (SNs) in blind cavefish Astyanax hubbsi and sighted river fish Astyanax mexicanus were ~150 and 42 µm, respectively. The cupula is able to enhance the drag of the neuromast by increasing the overall surface area of the neuromast. In addition, the biological cupula is composed of ~90% water, and its material composition (and especially the hydrophilicity and permeability characteristics) plays a critical role in signal transmission [19]. In certain fishes, the cupula also has long thin fibres that run along the length of the cupula (Fig. 1*b*) [20]. These fibres act as a scaffold that supports the cupula structure, thus allowing it to grow taller and away from the stagnant boundary layer of the surface of the fish [21], thereby increasing the aspect ratio of the overall sensory organs and their sensitivities. These fibres probably aid in coupling the hair cells to the hydrogel cupula as well, which facilitates the mechanotransduction process in transmitting the energy from cupula to the hair cells [18].

2.1.2 Pit organ: In non-teleost fishes and amphibians, some SNs that sit in pits or grooves on the skin are referred to be called as 'pit organs,' and linear series of such neuromasts are viewed as 'pit lines' [22–24]. Northcutt and Bleckmann [25] investigated that the 'pit organs' in the axolotl (*Ambystoma mexicanum*) are similar to other

Biosurf. Biotribol., 2020, Vol. 6, Iss. 1, pp. 12–19

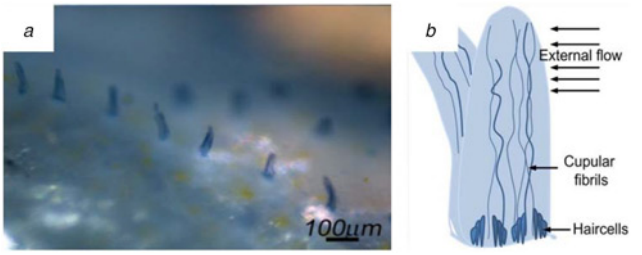

Fig. 1 *Morphology and schematic diagram of SN*

a Micrograph of the several cupulas (dark cylinders) of the SN row arrays [17]
b A schematic diagram of the cupula showing the basic morphology of the biological SN [20]

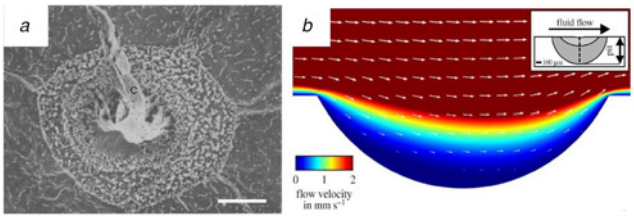

Fig. 2 *Morphology and CFD analysis results of pit organ*

a Pit organ in a three-week old axolotl larva [25]. Scale bar, 10 μm
b Exemplary flow field induced by a DC flow of 10 cm/s [26]

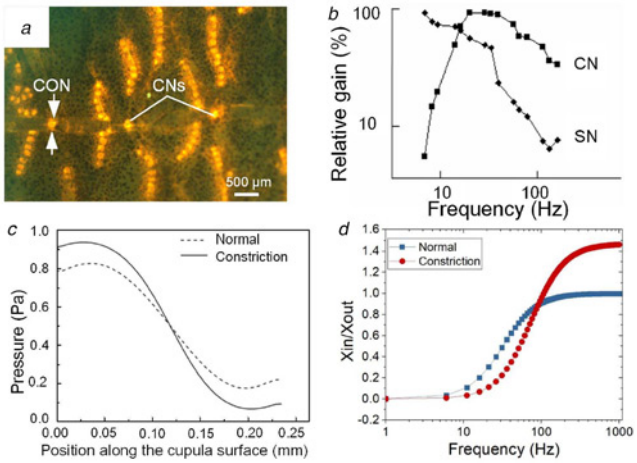

Fig. 3 *Morphology and function of canal lateral line*

a A fluorescence image of the trunk lateral-line system of Sinocyclocheilus microphthalmus [1]. CON, constriction microstructure
b Frequency response properties of superficial (SN) and canal (CN) neuromasts in the eel [27]
c Normal stress variation with the position along the cupula surface [11]
d Mechanical properties of the lateral-line canals with a length of 5 mm and a diameter of 0.4 mm. The red line with filled circles represents the constricted canal consisting of a wider canal with a length of 3 mm and diameter $d_1 = 0.4$ mm and a narrower canal with a length of 2 mm and diameter $d_2 = 0.24$ mm determined using (1)–(4)

neuromasts both morphologically and physiologically (Fig. 2*a*). Herzog *et al.* found that the ide *Leuciscus idus* has epidermal pits (indentations in the skin) in the anterior part of the head in addition to relatively small diameter cephalic lateral-line canals, varied in width and depth (from 30 μm × 30 μm to 80 μm × 60 μm) [26]. Their simulation results of CFD (computational fluid dynamics) revealed that the pits reduced the stimulation of the cephalic lateral-line system by bulk water flow (Fig. 2*b*), but did not attenuate the high-frequency water motions generated by a nearby dipole source appreciably, thus increasing the ratio between high-frequency local stimuli and background flow. In a natural environment, this would enable the animal to detect hydrodynamic signals generated, for instance, by prey or approaching predators even in the presence of strong background currents.

2.1.3 Lateral-line canal: As the mechanoreceptors in the lateral-line system, neuromasts in most teleost fish can be divided into two types: canal neuromasts (CNs) and SNs. Since SNs are freestanding on the skin surface, the cupula interacts with external fluids directly and is sensitive to flow velocities. In contrast to SNs, CNs are located in the subepidermal fluid-filled lateral-line canals connected to the ambient environment via canal pores and thus are sensitive to the pressure gradients between two adjacent canal pores [1]. The width of canals in the fish head ranges widely, from 0.1 to 2–3 mm. With respect to flow, SNs are low-pass filters encoding direct current (DC) flows and low-frequency oscillating flows of up to 10 s of Hz. In comparison, CNs do not respond to DC flows, but are sensitive to oscillating flows in the range of 10 to ~500 Hz (Fig. 3*b*) [27]. The essential idea is that CNs are less influenced by low-frequency large scale flows such as those generated by currents in the water surrounding the animal, or movements of the animal itself. This enables CNs to respond to the higher frequency signals generated by other animals.

2.1.4 Constriction microstructures: Canal morphology plays a crucial role in the sensitivity of the canal lateral-line system [1, 28]. In some fish species, the canal lateral-line systems possess constriction microstructures nearby the CNs [11, 29, 30]. Jiang *et al.* [11] discovered that the trunk canal lateral-line system in *Sinocyclocheilus macrophthalmus* and *S. microphthalmus* exhibited constriction microstructures nearby the CNs, with diameters of 216 and 210 μm, respectively. The results of flow-structure interaction simulation suggested that the constriction within the lateral-line canal could enhance the sensitivity of the canal lateral-line system (Fig. 3*c*).

A mathematical model for the lateral-line canal mechanics was proposed by Denton and Gray [31, 32]. They measured and modelled the fluid motions inside the actual lateral-line canals and canal-like structures (such as capillary tubes) as functions of the frequency of sinusoidal water motions outside the canal. The lateral-line canal was represented by a canal consisting of a circular section with diameter d_1, which contained a narrower circular section with diameter d_2 (their corresponding lengths were equal to l_1 and l_2, respectively). If X_{in}/X_{out} designates the ratio between the relative amplitudes of displacements in the narrower part of the canal and in the liquid adjacent to the canal, it can be found that

$$\frac{X_{in}}{X_{out}} = \frac{j\omega I_{out}}{j\omega I_{in} + R_{in}} \tag{1}$$

where $\omega = 2\pi f$, j is the complex operator, I_{out} and I_{in} are the inertances outside and inside the canal, respectively, which are calculated as follows:

$$I_{out} = \frac{\rho(l_1 + l_2)}{a_2} \tag{2}$$

$$I_{in} = \rho\left(\frac{l_1}{a_1} + \frac{l_2}{a_2}\right) \tag{3}$$

The frictional (viscous) resistance (R_{in}) under the steady (Hagen–Poiseuille) flow conditions, can be calculated as

$$R_{in} = 8\pi\eta\left(\frac{l_1}{a_1^2} + \frac{l_2}{a_2^2}\right) \tag{4}$$

where ρ is the density of the surrounding fluid ($\rho = 1000$ kg/m^3), and η is the dynamic viscosity ($\eta = 0.001$ Pa·s). As shown in Fig. 3*d*, the constriction microstructure within the lateral-line canal can result in: (i) further attenuation of the response at low frequencies;

(ii) an upward shift in the cut-off frequency; and (iii) higher sensitivity at higher frequencies [33].

2.2 Seal whiskers

Harbour seals are able to forage in low visibility environments, and even at depths >300 m. Their whiskers allow them to follow the vortices left by prey and detect objects that passed by even 30 s earlier [34]. Researchers have found that the microstructures of seal whiskers are able to reduce the vortex-induced vibration (VIV) and enhance their detection ability for wake [35].

2.2.1 Whisker morphology: Seal whiskers are longer and stiffer than those of other sea animals, and the follicles are surrounded by complex nerve fibres and a variety of mechanoreceptors. Lisa F. Shatz indicated that the length of the whiskers of harp seal, *Pagophilus Groenlandicus*, ranges from 0.8 to 10.5 cm and the diameter is on the order of tenths of millimetres. The mass density of the whiskers is 911 ± 100 kg/m^3, and Young's modulus ranges from 1.8 to 3.3 GPa [36]. Remarkably, the whiskers of harbour seals have a peculiar cross-sectional shape: the cross-section is elliptical, and the ratio of the major to minor axes varies along the whisker, with a period of ~1 to 3 mm, thus giving the whisker an undulated surface structure that distinguishes it from the whisker of eared seals, for instance, the sea lion (Fig. 4) [10, 37]. The microstructures of seal whiskers play an important role in the VIV reduction and enhancing wake detection.

2.2.2 Enhanced wake detection: A cylinder located in flow water will spontaneously generate a staggered double vortex array, known as Kármán vortices. The unsteady forces caused by Kármán vortices generate high-frequency VIV on the object. This vibration acts as a strong noise for the sensor, and it is difficult to discriminate between the wake-induced fluctuations and external flow unsteadiness [10]. The unique interfacial microstructures of the seal whisker can suppress VIVs, thereby reducing the noise produced by vibrating whiskers as the seal swims in the water [38]. Schulte-Pelkum *et al.* [39] noticed that when the seals were moving forward in the water, there was no noticeable difference in the posture of the whiskers compared to the posture in the air. The whiskers did not bend or vibrate obviously as it swam forward, suggesting that the seal whisker can effectively reduce its vibration, thereby improving its sensitivity to vortices left by upstream objects. The CFD simulation results of the wakes generated by seal whiskers revealed that Kármán vortices were replaced by a complex vortex structure in which various vortices were generated simultaneously in the direction of the whisker axis (Fig. 5*a*) [10]. Beem and Triantafyllou [40] used dye to capture a bottom-up view of wakes generated by various whiskers (Fig. 5*b*). Their results illustrated that the seal whisker was able to reduce VIV, which was in accordance with the simulation results. In addition, they found seal whiskers vibrated significantly more when they were in the wake of an upstream cylinder than they did

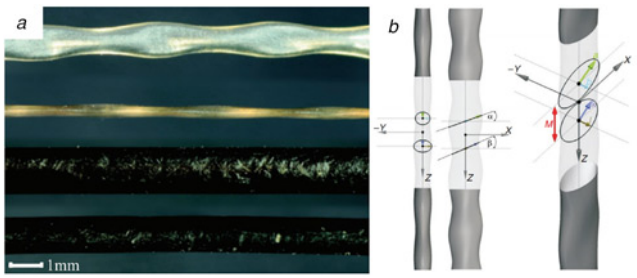

Fig. 4 *Microstructure of seal whisker [10]*

a Structure of harbour seal and California sea lion whiskers. Harbour seal whisker in dorsal and frontal views. Sea lion whisker in frontal and dorsal views
b Harbour seal whisker surface model

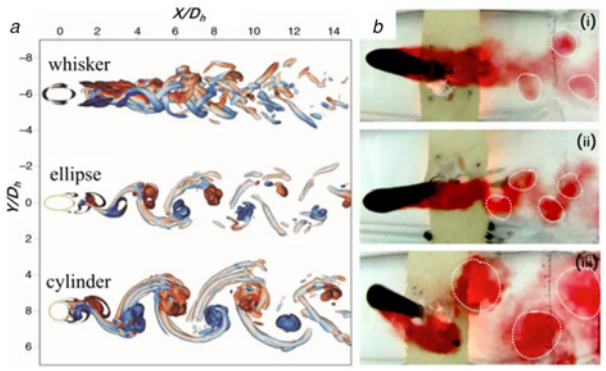

Fig. 5 *CFD simulation and dye staining results of the wakes generated by different whiskers*

a Numerical simulation of the wake-flow behind different cylinder bodies at the Reynolds numbers of 500 [10]
b The wake visualised using dye behind a whisker (i), elliptical cylinder (ii), and circular cylinder (iii) [40]

in bulk flow. By contrast, the circular cylinder vibrated with a similar amplitude for all cases even at the largest distance tested and the seal whisker amplitude was greater than its VIV amplitude. The results suggest that seal whiskers are highly sensitive as flow field sensors, especially for changing eddy current signals.

2.3 Flow-sensing hair in arthropods

Hair-like receptors are commonly found in crickets, cockroaches, spiders and scorpions serving as flow sensors [12, 41]. Among them, filiform hairs presented on the cricket's cerci and trichobothria appeared on the spider's leg are known as the most sensitive biological flow sensors [7, 42]. To elicit an action potential, the work needed to drive the hair shaft to deflect enough is on the order of 10^{-21} J for a cricket filiform hair, which corresponds to 1/100 of the energy of a single photon [43]. In addition, the size of the cricket's (*Gryllus bimaculatus*) filiform hair varies widely between 30–1500 µm in length and 1–9 µm in diameter at the base [43]. The Young's modulus of the cricket's filiform hair varies from 6 to 9 GPa and the mass density is 1100 kg/m^3 [44]. The size of the spider's (*Cupiennius salei*) trichobothria varies widely between 600–2600 µm in length and around 10 µm in diameter at the base, and Young's modulus is 4 GPa [42].

2.3.1 Lever system: All the flow-sensing hairs are located in a cup-mouth shape cuticular socket (Fig. 6) and the hair shaft forms a simple lever with the long arm exposed to the motion of airflow and the short arm embedded in the exoskeleton coupling with the sensory cells. The length ratio of the outer to inner arm is more than 1000/1 [8], which indicates that the displacement of the hair's tip is scaled down while the force is scaled up. Fig. 6 shows the schematic diagram of the flow-sensing hairs [42]. The inner end of the hair shaft couples with the dendrites and the viscoelastic suspension behaves as a combination of a spring and a dashpot,

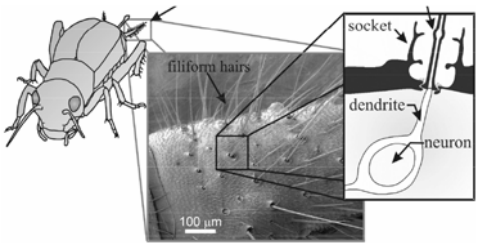

Fig. 6 *Filiform hairs in crickets [47]*

Biosurf. Biotribol., 2020, Vol. 6, Iss. 1, pp. 12–19

which resists the deflection of the hair shaft. As for the trichobothria in spider *Cupiennius Salei*, the spring stiffness is on the order of 10^{-11}–10^{-12} Nm/rad and the damping coefficient is on the order of 10^{-14}–10^{-15} Nms/rad [45, 46]. These extremely low values result in the pure tilt without bending when suffered from the viscous force of airflow [7].

2.3.2 Tapered and feathered structures: Tapering is a common feature in the multiple biological hairs [48]. By applying an equal point load at a cylindrical hair and a tapered hair with equal length and base diameter, the tapered hair deflects more than the cylindrical hair due to the relatively small stiffness, which indicates that a tapered hair's deflection capability has a steep gradient in sensitivity compared with a cylindrical hair. Dickinson investigated the sensitivity of flow-sensing hair including the tapered one and the cylindrical one (Fig. 7*a*) for the detection of changes in laminar boundary layer shape, and the simulated results demonstrated that the tapered hair shape showed relatively larger sensitivity than the cylindrical hair [49]. In addition, Kumagai *et al.* [50] present a similar 'square-root cone' shape to model the filiform hairs in the crickets and cockroaches. The mean shape index of the filiform hairs in crickets is calculated to be 1.91. When applying the shape index for the model of the flow-sensing hair, the sensitivity presents to be greater than that of a cylindrical shape, which indicates that the unique tapered shape of filiform hairs in cricket can indeed lead to enhanced sensitivity [49].

Furthermore, in some of the flow-sensing hairs such as the trichobothria of the spider *Cupiennius Salei*, the surface of the hair shaft is feathered (Fig. 7*b*) [8]. The feathered structure can enhance the drag force generated by the trichobothria and thus the sensitivity. This is because at Reynolds numbers of about 10^{-2}, the effect of air viscosity becomes dominated and the proximity of the branches works to arrest the motion of air between them. The existence of the branches enlarges the surface area and thus leads to an enlarged drag force [51].

2.3.3 Hair arrays: The flow-sensing hairs of arthropod work in array in most cases. As the flow-sensing hairs present various lengths in an array on the walking leg of spider *Cupiennius Salei* (Fig. 8), the array of the hairs covers a large range of frequency with high sensitivity compared to a single hair, which is experimentally verified by analysing the mechanical frequency responses of five neighbouring hairs [45]. Furthermore, the individual hairs in an array differ in the directional sensitivity [52], which has been reported to exist in cercal filiform hairs of cockroaches and crickets [53, 54]. Additionally, Cummins *et al.* [55] modelled and quantified the interaction between the filiform hairs in crickets and demonstrated that the interaction between hairs in an array is significant at biologically relevant distances and air velocities, which indicates that the sensitivity of the flow-sensing hairs can be modified by the arrays of relatively impermeable hairs.

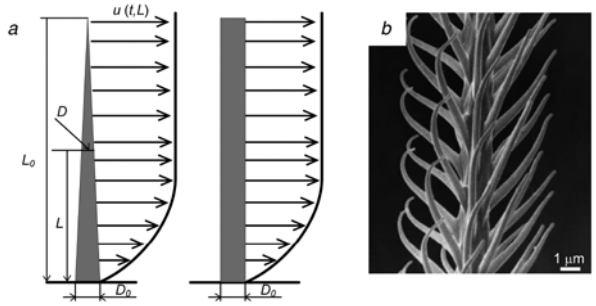

Fig. 7 *Illustration of the structure of flow-sensing hairs*

a Investigation of tapered (left) and cylindrical (right) flow-sensing hairs' sensitivity in laminar boundary layer
b Feathered structure of a trichobothria in the spider [8]

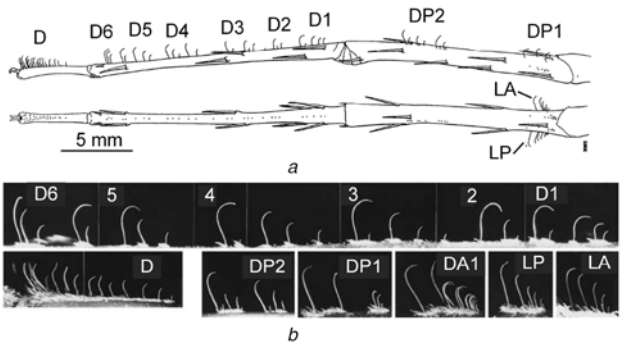

Fig. 8 *Arrangement of arrays of flow-sensing hairs*

a Dorsal and lateral views of the left second walking leg of spider *Cupiennius Salei* [45]
b Trichobothria in a higher magnification on different segments of the leg [45]

3 Underwater flow sensors with bio-inspired interfacial microstructures

To meet the challenge in hydrodynamic detection, biological flow receptors such as lateral line and seal whisker provide plenty of inspiration in the design of underwater flow sensors. The section describes the recent progress in ALL systems and whisker sensors.

3.1 ALL sensor

3.1.1 Hydrogel cilia for enhanced sensitivity: Inspired by the biological cupula, many researchers have developed various artificial hydrogel to improve the sensitivity of ALL sensor. Peleshanko *et al.* [56] firstly developed an ALL sensor with hydrogel cupula (Fig. 9*a*). The ALL sensor featuring silicon (Si) cantilever membrane and a standing polymer hair capped by hydrogel cupula. The minimum flow velocity detection limit was improved by over 2.5 times from 0.2 to 0.075 mm/s after capping the ALL sensor with hydrogel cupula. After that, they developed a higher aspect ratio cupula to improve the performance of the same MEMS (Micro-Electro-Mechanical System) piezoresistive ALL sensor, mimicking the properties of SN cupula (Fig. 9*b*) [17]. The oscillatory flow experimental results showed that the minimum velocity detection threshold was improved for 'bare' sensors from 0.1 to 0.0025 mm/s for sensors with hydrogel cilia.

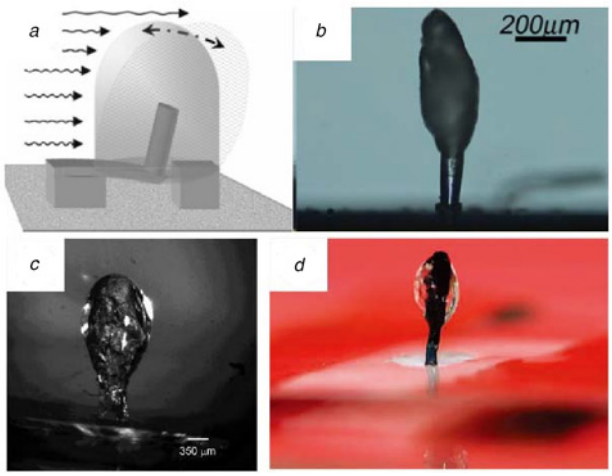

Fig. 9 *Various ALL sensors with hydrogel cilia*

a Hydrogel-capped hair flow sensor [56]
b Optimised ALL flow sensors with a high-aspect ratio biomimetic cupula [17]
c Hydrogel-dressed sensor containing the hydrogel cupula and encapsulated nanofibrils [20]
d A biomimetic flow sensor featuring a piezoelectric membrane with a hydrogel-infused VACNT bundle [57]

Miao and Triantafyllou from the Singapore MIT Alliance for Research and Technology developed various flexible ALL sensors based on the hydrogel cilia. In 2016, they proposed a canopy-like nanofibril pyramid around a Si60 polymer cilium by electrospinning and then drop-casted hydrogel cupula on the nanofibril scaffold (Fig. 9*c*) [20]. The comparative experimental study conducted to evaluate the sensitivities of the naked hair cell sensor and the cupula-dressed sensor in sensing steady-state flows demonstrated a sensitivity enhancement by 3.5–5 times due to the presence of hydrogel cupula. In 2017, they reported a biomimetic nanoelectromechanical system ALL sensor featuring a polyvinylidene fluoride (PVDF) nanofibre sensing membrane with a hydrogel infused, vertically aligned carbon nanotube (VACNT) bundle that mechanically interacts with the flow (Fig. 9*d*) [57]. The hydrodynamic experimental flow characterisation results revealed that the contributions of the mechanical and structural properties of the hydrogel in offering a sensing performance superior to that of conventional sensors.

3.1.2 Canal morphology for pressure sensing: Inspired by the canal lateral line in fish, various canal ALL sensors were proposed. In 2011, Bleckmann *et al.* [58] proposed a canal ALL for hydrodynamic detection using previously reported piezoresistive biomimetic superficial ALL sensors and PDMS (polydimethylsiloxane) canals, and its noise-rejection capability was revealed (Fig. 10*a*). In 2014, Kottapalli *et al.* [59] presented a MEMS canal ALL sensor by integrating liquid crystal polymer MEMS sensing membranes, high-aspect ratio Si60 pillars, and a PDMS canal. The experimental results demonstrated that the canal structure completely filtered away from the DC flow at all flow velocities ranging from 0 to 275 mm/s. In 2015, they reported another artificial MEMS canal ALL sensor based on a piezoelectric MEMS sensing membrane, revealing that the canal ALL sensor could reject the noises generated by the DC and low-frequency alternating current flows [60]. In 2017, Jiang *et al.* [61] developed a canal ALL sensor by integrating cantilevered flow-sensing elements in a PDMS canal (Fig. 10*b*), which demonstrated high-pass filtering capabilities to attenuate low-frequency stimuli.

Mimicking the constriction structure in the canal, Herzog *et al.* [62] proposed a new canal ALL sensor by placing light-guided PDMS lamella into a canal with constriction structure (Fig. 10*c*). The experimental results showed that the canal ALL sensor was able to detect a fluid flow velocity of 185 μm/s inside the canal. In 2019, Ma *et al.* [63] proposed a flexible canal ALL based on the organic piezoelectric film, with constriction structure nearby the sensing element (Fig. 10*d*). Their characterisation results revealed that the constriction structure can: (i) enhance the sensitivity of canal ALL sensor; (ii) modify the frequency response of the canal ALL sensor.

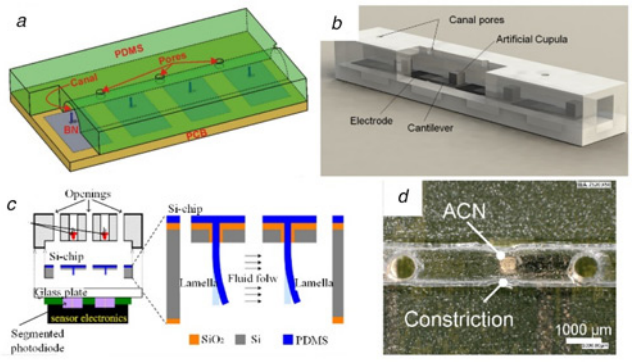

Fig. 10 *Various canal ALL sensors*

a A diagram illustrating the structural details of the canal ALL sensor [58]
b Flexible canal ALL sensor [61]
c Canal ALL sensor with optical sensing mechanism [62]
d Flexible canal ALL sensor with constriction structure [63]

3.2 Artificial seal whisker sensor

Since the undulatory and asymmetric geometry of the seal whisker can suppress VIVs and increase the signal-to-noise ratio in hydrodynamic detection, various artificial seal whisker sensors have been developed to provide underwater vehicles with a 'feel' of the surrounding flow. Beem *et al.* [64] developed a low-cost artificial seal whisker sensor by utilising flow flexpoint bend sensors at the base of a whisker model as shown in Fig. 11*a*. It could detect its angle of attack in a passive manner and determine the flow velocity and direction. Compared with a circular rod in place of the harbour seal whisker geometry, the artificial seal whisker sensor showed enhanced sensing performance to distinguish self-induced vibration from the vibration induced by oncoming wake features. Kottapalli *et al.* [65] presented a novel design and fabrication of a bio-inspired artificial whisker sensor using a piezoelectric MEMS sensing membrane and a polymer micro-whisker fabricated by stereolithography process as shown in Fig. 11*b*.

With a strong demand for wake information detection, researchers devoted to developing artificial whisker sensors with new transduction mechanism. For example, Eberhardt *et al.* [66] developed a capacitive-type artificial whisker using a cone-in-cone based design with conductive material creating parallel-plate capacitors. The sensor prototype was mounted on a captive harbour seal adjacent to its own whisker array, showing the possibility to track a remote-controlled submarine. With the aim of soft robotic applications, Gul *et al.* [67] demonstrated a fully 3D printed multi-material whisker sensor, composed of a polyurethane rod a four graphene patterns as piezoresistors.

4 Airflow sensors with bio-inspired interfacial microstructures

Airflow sensing is an essential technique involved in diverse applications, such as traditional flow mapping, manoeuvring system of self-stabilising micro air vehicles (MAVs) and real-time monitoring of meteorological information. Various transduction mechanisms, such as thermal [68], piezoresistive [69], piezoelectric [70], capacitive [71], magnetic [72] and optical, have been used in the development of airflow sensors. In this section, the research status on the development of airflow sensors with bio-inspired interfacial microstructures is provided. Moreover, the airflow sensor array for vectorial sensing and the coupling of hair-like structures are also discussed.

4.1 Hair-like airflow sensors

Inspired by the sensing principles of hair-like receptors in arthropods, hair-like structures have been widely used to develop various airflow sensors with the principle of shaft or cantilever

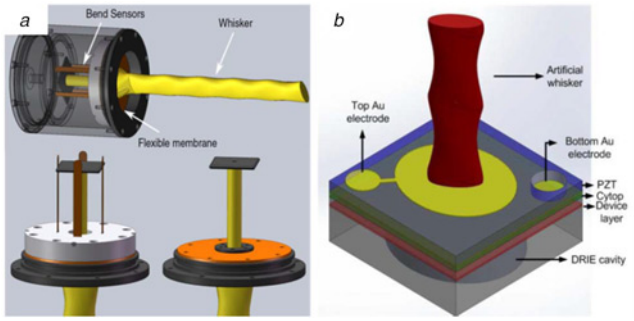

Fig. 11 *Artificial seal whisker sensors*

a Piezoresistive artificial seal whisker sensor [64]
b Piezoelectric artificial seal whisker sensor [65]

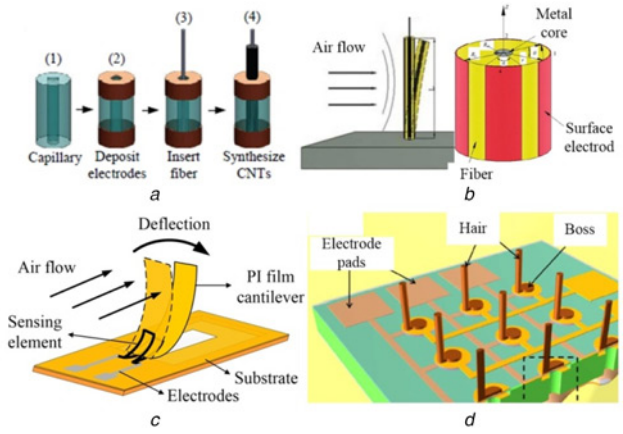

Fig. 12 *Hair-like airflow sensors*

a Carbon nanotube fuzzy fibre-type airflow sensor [73]
b Piezoelectric fibre-type airflow sensor [74]
c Piezoresistive cantilever-type airflow sensor [75]
d Capacitive-type airflow sensor array [77]

deflection caused by airflow. Using the piezoresistive effect as the operation principle, Maschmann *et al.* [73] adopted artificial hair sensors based on structural glass fibres coated with a radially aligned forest of carbon nanotubes (CNTs) for omni-directional detection of low-speed airflow (Fig. 12*a*). Based on piezoelectric transduction mechanism, a multi-electrode metal-core piezoelectric fibre-based structure has been designed to enhance the performance of the airflow sensor [74]. The longitudinal surface of the piezoelectric ceramic is coated symmetrically with four thin metal layers. The fabricated airflow sensor can obtain the magnitude and direction of airflow (Fig. 12*b*). Furthermore, cantilever-type and flag-type flow sensors have been demonstrated. Jiang *et al.* [75] proposed an all-polymer flexible airflow sensor using a self-bending cantilever (Fig. 12*c*). The fabricated airflow sensor presents a high resolution (~0.5 m/s), a large detection range (0–20 m/s), and good repeatability. Yu-Hsiang *et al.* [76] fabricated an MEMs-based airflow sensor with a flag-type free-standing micro-cantilever structure. Fig. 12*d* illustrates a new type of low-power, accurate and robust flow sensor in which a hair-like appendage was used to translate flow into hydraulic pressure [77]. The pressure was amplified and sensed with a capacitance that was integrated with the micro-hydraulic system.

Inspired by the thrips wing, a comb-like cantilever-based pressure sensor was developed [78]. The overlapping of the comb structure was designed to decrease the air leak from the gap between the cantilever and the surrounding frame. The air leakage of the fabricated comb-like cantilever was smaller than that of the normal cantilever when the differential pressure was over 40 Pa, whereas the sensitivity to constant differential pressure was equal to each other. To detect minute airflow motions, the pappus-type sensor was developed to increase the drag force on the cantilever tip [79]. Experimental results indicated that hundreds of hairs of the pappus increased the sensitivity of the sensor by increasing the drag at the tip.

In recent years, hair-like airflow sensor array has been employed to achieve vectorial sensing capability. For instance, Ma *et al.* [80] developed an MEMS-based low-cost sensing platform for sensing airflow velocity and flow direction comprising four silicon nitride cantilever beams arranged in across-form configuration (Fig. 13*a*). The experimental results have confirmed that the resulting variation in the output signals of the integrated sensors can be used to determine not only the ambient temperature and the velocity of the airflow, but also its direction relative to the sensor with an accuracy of ±7.5°. As shown in Fig. 13*b*, a ring array design, which was composed of eight PVDF micro-cantilevers, was proposed to determine the airflow velocity and direction effectively [81].

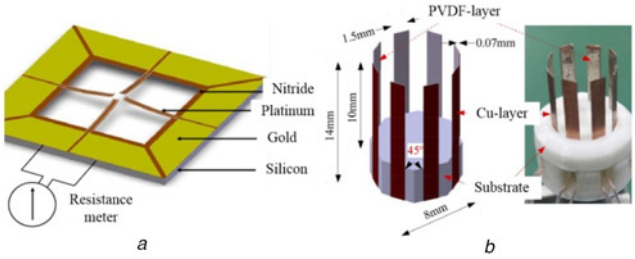

Fig. 13 *Airflow sensor array for vectorial sensing*

a Airflow sensor comprising of four cantilever beams [80]
b Ring sensor array with eight PVDF micro-cantilevers [81]

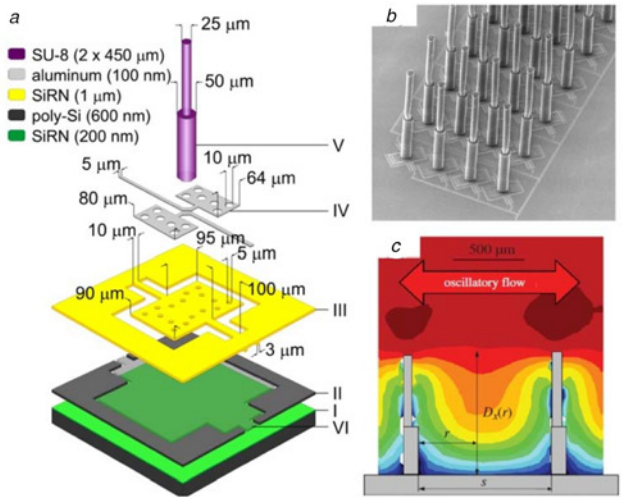

Fig. 14 *Airflow sensor array designed by Twente*

a A schematic drawing of such sensor [82]
b Fabricated sensor array [83]
c PIV measurement of a pair of hairs [84]

4.2 Viscous coupling of hair-like structures

Inspired by cerci of crickets, capacitive-type airflow sensor array was developed in the University of Twente. In their design, each artificial hair is situated at the centre of a suspended membrane and a capacitor is formed by the top electrodes deposited on the suspended membrane and the bottom electrode deposited on the base of the substrate [82]. Flow-induced tilting of the hair is resisted by the torsional stiffness of the membrane, whose deflection will result in a change of the capacitances of the sensor (Fig. 14*a*). An example of a fabricated sensor array is illustrated in Fig. 14*b* [83].

To study the hydrodynamic coupling between densely packed flow-sensitive hairs, the extent of flow perturbation by single and tandem hairs has been quantified using biomimetic MEMS hairs as physical models and particle image velocimetry (PIV) for flow visualisation [84]. PIV measurements provide two-dimensional flow velocities in the cross-section of a pair of hairs arranged in tandem, with frequency and inter-hair distances as variables, as shown in Fig. 14*c*. The results suggest that reduced inter-hair distances lead to increased phase shifts between the far-field flow and the flow measured between two hairs. The fact confirmed that viscous coupling was particularly strong for low-frequency flows. With a high density of hairs, the airflow sensor array is most likely to work as a dynamically coupled set of resonators.

5 Conclusion and outlook

In summary, sensing-enhancement mechanisms are ubiquitous in biological flow perception systems, such as lateral-line system of

Table 1 Summary of the biomechanical mechanism and the artificial flow sensors

Biological prototype	Biomechanical mechanism	Artificial flow sensors			
		Size of structure, μm	Material of structure	Performance parameters	Ref.
lateral-line canal	high-pass filter	Cantilever: 5000 (L) × 2000 (W) × 86 (T) Cupula: Cubic side length 1500	Cupula: PDMS Cantilever: PVDF/ polypropylene Canal: PDMS	attenuate low-frequency stimulus 11 Pa/m (@ 115 ± 1 Hz)	[60]
constriction within lateral-line canal	velocity-enhancement	Cantilever: 1000 (L) × 500 (W) × 12 (T) Cupula: 500 (H) × 300 (D) Constriction: 700 (W) Canal: 1000 (W)	Cupula: PDMS Cantilever: PVDF/ polypropylene Canal: PDMS	0.64 Pa/m	[63]
cupula within neuromast	drag-enhancement	Hydrogel cupula: 2700 (H) × 1000 (D)	Cupula: Hyaulronic acid-based hydrogel (E:10–100 Pa)	S: 77 mV/m/s R: 0.018 m/s sensitivity enhancement by 3.5–5 times	[20]
asymmetric geometry of the seal whiskers	suppressing VIVs	—	Whiskers: Si60 polymer	velocity detection limit as low as 193 μm/s.	[65]
lever system of filiform hairs on crickets	suspended hair model	Hair: 900 (L) × 44 (D) Membrane: 95(L) × 90 (W)	Hair: SU-8 Membrane: Si_xN_y	detection limit: 5 mm/s (@30 Hz flow frequency)	[83]
array of trichobothria on spiders	different directional sensitivity	Cantilever: 4000 (L) × 400 (W) × 1 (T)	Cantilever: Si_3N_4	Accuracy: ± 7.5°	[80]

L: length; W: width; T: Thickness; H: height; D: diameter; S: sensitivity; R: resolution.

fish, harbour seal whisker, and filiform hair of cricket. The interfacial microstructures play an important role in increasing the sensitivity, reducing the noise level, or modifying the frequency response of flow receptors. Inspired by the interesting sensing-enhancement mechanisms, researchers developed various novel flow sensors varying from ALL sensor with constriction canals, artificial seal whiskers with undulatory geometry, to hair-type airflow sensors, as is shown in Table 1. However, it should be mentioned that most of these sensors are in the prototype phase and have not gained success in industries. In addition to learning from the nature in biomechanics, the sensor engineers should combine the bio-inspired principles with superior MEMS technology to achieve high-sensitive, wide working range, and low-cost engineered sensor systems.

6 Acknowledgments

This work was financially supported by the National Natural Science Foundation of China (grant no. 51575027 and 51975030).

7 References

[1] Jiang, Y., Ma, Z., Zhang, D.: 'Flow field perception based on the fish lateral line system', *Bioinspiration Biomimetics*, 2019, **14**, p. 041001
[2] Brown, R.E., Fedde, M.R.: 'Airflow sensors in the avian wing', *J. Exp. Biol.*, 1993, **179**, pp. 13–30
[3] Rinberg, D., Davidowitz, H.: 'Do cockroaches 'know' about fluid dynamics?', *Nature*, 2000, **405**, pp. 756–756
[4] Stacconi, V. R., Romani, R.: 'The Johnston's organ of three homopteran species: a comparative ultrastructural study', *Arthropod Struct. Dev.*, 2013, **42**, pp. 219–228
[5] Dehnhardt, G., Mauck, B., Hanke, W., *et al.*: 'Hydrodynamic trail-following in harbor seals (Phoca vituline)', *Science*, 2001, **293**, pp. 102–104
[6] Englmann, J., Hanke, W., Mogdans, J., *et al.*: 'Hydrodynamic stimuli and the fish lateral line', *Nature*, 2000, **408**, pp. 51–52
[7] Fratzl, P., Barth, F.G.: 'Biomaterial systems for mechanosensing and actuation', *Nature*, 2009, **462**, pp. 442–448
[8] Humphrey, J.A.C., Barth, F.G.: 'Medium flow-sensing hairs: biomechanics and models', *Adv. In Insect Phys.*, 2007, **34**, pp. 1–80
[9] Dehnhardt, G., Mauck, B., Bleckmann, H.: 'Seal whiskers detect water movements', *Nature*, 1998, **394**, pp. 235–236
[10] Hanke, W., Witte, M., Miersch, L., *et al.*: 'Harbor seal vibrissa morphology suppresses vortex-induced vibrations.', *J. Exp. Biol.*, 2010, **213**, pp. 2665–2672
[11] Jiang, Y.G., Fu, J.C., Zhang, D.Y., *et al.*: 'Investigation on the lateral line systems of two cave fish: Sinocyclocheilus macrophthalmus and S. Microphthalmus (Cypriniformes: Cyprinidae)', *J Bionic. Eng.*, 2016, **13**, pp. 108–114
[12] Han, Z., Liu, L., Wang, K., *et al.*: 'Artificial hair-like sensors inspired from nature: a review', *J. Bionic. Eng.*, 2018, **15**, pp. 409–434
[13] Triantafyllou, M.S., Weymouth, G.D., Miao, J.: 'Biomimetic survival hydrodynamics and flow sensing', *Annu. Rev. Fluid Mech.*, 2016, **48**, pp. 1–24
[14] Mohamed, A., Watkins, S., Clothier, R., *et al.*: 'Fixed-wing MAV attitude in atmospheric turbulence-part 2: investigating biologically-inspired sensors', *Prog. Aerosp. Sci.*, 2014, **71**, pp. 1–13
[15] Bleckmann, H.: 'Reception of hydrodynamic stimuli in aquatic and semiaquatic animals' (Gustav Fischer Verlag, Stuttgart, 1994)
[16] Coombs, S., Montgomery, J.: 'The enigmatic lateral line system', *Comparative Hearing, Fish and Amphibians*, 1999, **11**, pp. 319–362
[17] McConney, M.E., Chen, N., Lu, D., *et al.*: 'Biologically inspired design of hydrogel-capped hair sensors for enhanced underwater flow detection', *Soft Mat.*, 2009, **5**, pp. 292–295
[18] Teyke, T.: 'Morphological differences in neuromasts of the blind cave fish Astyanax hubbsi and the sighted river fish Astyanax mexicanus', *Brain Behavior and Evolution.*, 1990, **35**, pp. 23–30
[19] McConney, M.E., Anderson, K.D., Brott, L.L., *et al.*: 'Bioinspired material approaches to sensing', *Adv. Funct. Mater.*, 2009, **19**, pp. 2527–2544
[20] Kottapalli, A.G.P., Bora, M., Asadnia, M., *et al.*: 'Nanofibril scaffold assisted MEMS artificial hydrogel neuromasts for enhanced sensitivity flow sensing', *Sci. Rep.*, 2016, **6**, p. 19336
[21] Anderson, K.D., Lu, D., McConney, M.E., *et al.*: 'Hydrogel microstructures combined with electrospun fibers and photopatterning for shape and modulus control', *Polymer*, 2008, **49**, pp. 5284–5293
[22] Lekander, B.: 'The sensory line system and the canal bones in the head of some Ostariophysi', *Acta Zoologica (Stockholm)*, 1949, **30**, pp. 1–131
[23] Nelson, G. J.: 'Cephalic sensory canals, pitlines, and the classification of esocoid fishes, with notes on galaxiids and other teleosts', *Am. Mus. Novitates*, 1972, **2492**, pp. 1–49
[24] Song, J., Northcutt, R.G.: 'Morphology, distribution and innervation of the lateral-line receptors of the Florida gar, Lepisosteus platyrhincus', *Brain Behav. Evol.*, 1991, **37**, pp. 10–37
[25] Northcutt, R.G., Bleckmann, H.: 'Pit organs in axolotls: A second class of lateral line neuromasts', *J.Comparative Physiol. A*, 1993, **172**, pp. 439–446
[26] Herzog, H., Klein, B., Ziegler, A.: 'Form and function of the teleost lateral line revealed using three-dimensional imaging and computational fluid dynamics', *J. R. Soc., Interface*, 2017, **14**, p. 20160898
[27] Voigt, R., Carton, A.G., Montgomery, J.C.: 'Responses of lateral line afferent neurones to water flow', *J. Exp. Biol.*, 2000, **203**, pp. 2495–2502
[28] Kaldenbach, F., Klein, A., Bleckmann, H.: 'Form-function relationship in artificial lateral lines', *Bioinspiration Biomimetics*, 2019, **14**, p. 026001
[29] Carton, A.G., Montgomery, J.C.: 'A comparison of lateral line morphology of blue cod and torrent fish: two sandperches of the family Pinguipedidae', *Evol. Biol. Fish.*, 2004, **70**, pp. 123–131
[30] Montgomery, J., Coombs, S., Janssen, J.: 'Form and function relationships in lateral line systems: comparative data from six species of antarctic notothenioid fish', *Brain Behav. Evol.*, 1994, **44**, pp. 299–306
[31] Denton, E.J., Gray, J.A.B.: 'Mechanical factors in the excitation of clupeid lateral lines', *Proc. R. Soc. B*, 1983, **218**, pp. 1–26
[32] Denton, E.J., Gray, J.A.B.: 'Mechanical factors in the excitation of the lateral line of fishes', in 'Sensory biology of aquatic animals' (Springer, New York, 1988), pp. 595–617
[33] Coombs, S., Netten, S.M.: 'The hydrodynamics and structural mechanics of the lateral line system', *Fish Physiol.*, 2005, **23**, pp. 103–139
[34] Dehnhardt, G., Mauck, B., Hanke, W., *et al.*: 'Hydrodynamic trail-following in harbor seals (Phoca vitulina)', *Science*, 2001, **293**, pp. 102–104
[35] Marshall, C.D., Amin, H., Kovacs, K.M., *et al.*: 'Microstructure and innervation of the mystacial vibrissal follicle-sinus complex in bearded seals, erignathus barbatus (pinnipedia: phocidae)', *Anat Rec A Discov. Mol Cell Evol. Biol.*, 2010, **288**, pp. 13–25
[36] Shatz, L.F., De Groot, T.: 'The frequency response of the vibrissae of harp seal, Pagophilus Groenlandicus, to sound air and water', *Plos ONE*, 2013, **8**, p. e54867

[37] Miersch, L., Hanke, W., Wieskotten, S., *et al*.: 'Flow sensing by pinniped whiskers', *Philos. Trans. R. Soc., B, Biol. Sci.*, 2011, **366**, pp. 3077–3084

[38] GlSer, N., Wieskotten, S., Otter, C., *et al*.: 'Hydrodynamic trail following in a California sea lion (Zalophus californianus)', *J.Comparative Physiol. A*, 2011, **197**, pp. 141–151

[39] Schulte-Pelkum, N., Wieskotten, S., Hanke, W., *et al*.: 'Tracking of biogenic hydrodynamic trails in harbour seals (Phoca vitulina)', *J. Exp. Biol.*, 2007, **210**, pp. 781–787

[40] Beem, H.R., Triantafyllou, M.S.: 'Wake-induced slaloming response explains exquisite sensitivity of seal whisker-like sensors', *J. Fluid Mech.*, 2015, **783**, pp. 306–322

[41] Humphrey, J.A.C., Devarakonda, R., Iglesias, I., *et al*.: 'Dynamics of arthropod filiform hairs. I. Mathematical modelling of the hair and air motions', *Phil. Trans. R. Soc. B.*, 1993, **340**, pp. 423–444

[42] Barth, F.G.: 'Spider mechanoreceptors', *Curr. Opin. Neurobiol.*, 2004, **14**, pp. 415–422

[43] Shimozawa, T., Murakami, J., Kumagai, T.: 'Cricket wind receptors: thermal noise for the highest sensitivity known', Barth, F.G., Humphrey, J.A.C., Secombin, T.W. (eds): *Sensors Sens. Biol. Eng.* (Springer, Vienna, 2003), pp. 145–157

[44] Joshi, K.: 'biomechanical analysis of a cricket filiform hair socket under low velocity air currents'. M.S. thesis, Montana State University, Bozeman, MT

[45] Barth, F.G., Wastl, U., Humphrey, J.A.C., *et al*.: 'Dynamics of arthropod filiform hairs. II. Mechanical properties of spider trichobothria (Cupiennius salei keys.)', *Philos. Trans. R. Soc. London. Ser. B Biol. Sci.*, 1993, **340**, pp. 445–461

[46] McConney, M.E., Schaber, C.F., Julian, M.D., *et al*.: 'Surface force spectroscopic point load measurements and viscoelastic modelling of the micromechanical properties of air flow sensitive hairs of a spider (Cupiennius salei)', *J. R. Soc. Interface.*, 2009, **6**, pp. 681–694

[47] Krijnen, G., Lammerink, T., Wiegerink, R., *et al*.: 'Cricket inspired flow-sensor arrays', Proc. of the IEEE Sensors, Atlanta, GA, USA, 2007, pp. 539–546

[48] Seale, M., Cummins, C., Viola, I.M., *et al*.: 'Design principles of hair-like structures as biological machines', *J. R. Soc. Interface.*, 2018, **15**, p. 20180206

[49] Dickinson, B.T.: 'Hair receptor sensitivity to changes in laminar boundary layer shape', *Bioinspiration and Biomimetics.*, 2010, **5**, p. 016002

[50] Kumagai, T., Shimozawa, T., Baba, Y.: 'The shape of wind-receptor hairs of cricket and cockroach', *J. Comp. Physiol., A Sensory, Neural, Behav. Physiol.*, 1998, **183**, pp. 187–192

[51] Barth, F.G.: 'How to catch the wind: spider hairs specialized for sensing the movement of air', *Naturwissenschaften*, 2000, **87**, pp. 51–58

[52] Dechant, H.E., Hößl, B., Rammerstorfer, F.G., *et al*.: 'Arthropod mechanoreceptive hairs: modeling the directionality of the joint', *J. Comp. Physiol. A.*, 2006, **192**, pp. 1271–1278

[53] Landolfa, M.A., Jacobs, G.A.: 'Direction sensitivity of the filiform hair population of the cricket cereal system', *J. Comp. Physiol. A.*, 1995, **177**, pp. 759–766

[54] Magal, C., Dangles, O., Caparroy, P., *et al*.: 'Hair canopy of cricket sensory system tuned to predator signals', *J. Theor. Biol.*, 2006, **241**, pp. 459–466

[55] Cummins, B., Gedeon, T., Klapper, I., *et al*.: 'Interaction between arthropod filiform hairs in a fluid environment', *J. Theor. Biol.*, 2007, **247**, pp. 266–280

[56] Peleshanko, S., Julian, M.D., Ornatska, M., *et al*.: 'Hydrogel-encapsulated microfabricated haircells mimicking fish cupula neuromast', *Adv. Mater.*, 2007, **19**, pp. 2903–2909

[57] Bora, M., Kottapalli, A.G.P., Miao, J., *et al*.: 'Biomimetic hydrogel-CNT network induced enhancement of fluid-structure interactions for ultrasensitive nanosensors', *NPG Asia Mater.*, 2017, **9**, p. e440

[58] Yang, Y.C., Klein, A., Bleckmann, H., *et al*.: 'Artificial lateral line canal for hydrodynamic detection', *Appl. Phys. Lett.*, 2011, **99**, p. 023701

[59] Kottapalli, A.G.P., Asadnia, M., Miao, J., *et al*.: 'Touch at a distance sensing: lateral-line inspired MEMS flow sensors', *Bioinspiration Biomimetics.*, 2014, **9**, p. 046011

[60] Asadnia, M., Kottapalli, A.G.P., Miao, J., *et al*.: 'Artificial fish skin of self-powered micro-electromechanical systems hair cells for sensing hydrodynamic flow phenomena', *J. R. Soc. Interfaces*, 2015, **12**, p. 20150322

[61] Jiang, Y., Ma, Z., Fu, J., *et al*.: 'Development of a flexible artificial lateral line canal system for hydrodynamic pressure detection', *Sensors*, 2017, **17**, p. 1220

[62] Herzog, H., Klein, A., Bleckmann, H., *et al*.: 'μ-biomimetic flow sensors-introducing light-guided PDMS structures into MEMS', *Bioinspiration Biomimetics*, 2015, **10**, p. 036001

[63] Ma, Z., Jiang, Y., Wu, P., *et al*.: 'Constriction canal assisted artificial lateral line system for enhanced hydrodynamic pressure sensing', *Bioinspiration Biomimetics*, 2019, **14**, p. 066004

[64] Beem, H., Hildner, M., Triantafyllou, M.: 'Calibration and validation of a harbor seal whisker-inspired flow sensor', *Smart Mater. Struct.*, 2013, **22**, p. 014012

[65] Kottapalli, A.G.P., Asadnia, M., Hans, H., *et al*.: 'Harbor seal inspired MEMS artificial micro-whisker sensor'. IEEE 27th Int. Conf. on Micro Electro Mechanical Systems (MEMS), San Francisco, CA, USA, 2014

[66] Eberhardt, W.C., Wakefield, B.F., Murphy, C.T., *et al*.: 'Development of an artificial sensor for hydrodynamic detection inspired by a seal's whisker array', *Bioinspiration Biomimetics*, 2016, **11**, p. 056011

[67] Gul, J.Z., Su, K.Y., Choi, K.H.: 'Fully 3D printed multi-material soft bio-inspired whisker sensor for underwater-induced vortex detection', *Soft Robot.*, 2018, **5**, pp. 122–132

[68] Sadeghi, M.M., Peterson, R.L., Najafi, K.: 'Air flow sensing using micro-wire-bonded hair-like hot-wire anemometry', *J. Micromech. Microeng.*, 2013, **23**, p. 085017

[69] Slinker, K.A., Kondash, C., Dickinson, B.T.: 'CNT-based artificial hair sensors for predictable boundary layer air flow sensing', *Adv. Mater. Technol.*, 2016, **1**, p. 1600176

[70] Tao, J., Yu, X., Berilla, J.: 'Bio-inspired flow and acoustic sensor'. Proc. SPIE, Orlando, FL, USA, 2011, vol. 8019, p. 80190R

[71] Krijinen, G., Floris, A.: 'Biomimetic micromechanical adaptive flow-sensor arrays', Proc. of SPIE, Maspalomas, Spain, 2007, vol. 6592, p. 65920F

[72] Alfadhel, A., Khan, M.A., Cardoso, S., *et al*.: 'A magnetoresistive tactile sensor for harsh environment applications', *Sensors*, 2016, **16**, p. 650

[73] Maschmann, M.R., Ehlert, G.J., Dickinson, B.T., *et al*.: 'Bioinspired carbon nanotube fuzzy fiber hair sensor for air-flow detection', *Adv. Mater..*, 2014, **26**, pp. 3230–3234

[74] Bian, Y., Zhang, Y., Xia, X.: 'Design and fabrication of a multi-electrode metal-core piezoelectric fiber and its application as an airflow sensor', *J. Bionic. Eng.*, 2016, **13**, pp. 416–425

[75] Jiang, Y., Shen, D., Liu, M., *et al*.: 'Fabrication of graphene/polyimide nanocomposite-based hair-like airflow sensor via direct inkjet printing and electrical breakdown', *Smart Mater. Struct.*, 2019, **28**, p. 065028

[76] Yu-Hsiang, W., Chia-Yen, L., Che-Ming, C.: 'A MEMS-based air flow sensor with a free-standing micro-cantilever structure', *Sensors*, 2007, **7**, pp. 2389–2401

[77] Sadeghi, M.M., Peterson, R.L., Najafi, K.: 'Micro-hydraulic structure for high performance bio-mimetic air flow sensor arrays'. Int. Electron Devices Meeting, Washington, DC, USA, 2011

[78] Takahashi, H., Isozaki, A., Matsumoto, K., *et al*.: 'A cantilever with comb structure modeled by a bristled wing of thrips for slight air leak'. Proc. of the IEEE Int. Conf. on Micro ElectroMechanical Systems (MEMS), Estoril, Portugal, 2015, pp. 706–709

[79] Bruecker, C.H., Vladimir, M., Vanesa, M.: 'Sensing of minute airflow motions near walls using pappus-type nature-inspired sensors', *PLOS ONE*, 2017, **12**, p. 0179253

[80] Ma, R.H., Wang, D.A., Hsueh, T.H., *et al*.: 'A MEMS-based flow rate and flow direction sensing platform with integrated temperature compensation scheme', *Sensors*, 2009, **9**, pp. 5460–5476

[81] Hu, J., Peng, H.: 'Design of PVDF sensor array for determining airflow direction and velocity', *Rev. Sci. Instrum.*, 2018, **89**, p. 085007

[82] Dagamseh, A.M.K., Lammerink, T.S.J., Sanders, R., *et al*.: 'Towards high-resolution flow cameras made of artificial hair flow-sensors for flow pattern recognition'. IEEE Int. Conf. on Micro Electro Mechanical Systems (MEMS), Cancun, Mexico, 2011

[83] Droogendijk, H., Bruinink, C.M., Sanders, R., *et al*.: 'Tunable sensor response by voltage-control in biomimetic hair flow sensors', *Micromachines.*, 2013, **4**, pp. 116–127

[84] Casas, J., Steinmann, T., Krijnen, G.: 'Why do insects have such a high density of flow-sensing hairs? Insights from the hydromechanics of biomimetic MEMS sensors', *J. R. Soc., Interface*, 2010, **7**, pp. 1487–1495